

Mechanics and wrinkling patterns of pressurized bent tubes

César L. Pastrana,¹ Luyi Qiu,² John W. Hutchinson,² Ariel Amir,^{2,3} and Ulrich Gerland¹

¹*Physics of Complex Biosystems, Technical University of Munich, 85748 Garching, Germany*

²*John A. Paulson School of Engineering and Applied Sciences,*

Harvard University, Cambridge, Massachusetts 02138, USA

³*Department of Physics of Complex Systems, Weizmann Institute of Science, 7610001 Rehovot, Israel*

Take a drinking straw and bend it from its ends. After sufficient bending, the tube buckles forming a kink, where the curvature is localized in a very small area. This instability, known generally as the Brazier effect, is inherent to thin-walled cylindrical shells, which are particularly ubiquitous in living systems, such as rod-shaped bacteria. However, tubular biological structures are often pressurized, and the knowledge of the mechanical response upon bending in this scenario is limited. In this work, we use a computational model to study the mechanical response and the deformations as a result of bending pressurized tubes. In addition, we employ tension-field theory to describe the mechanical behaviour before and after the wrinkling transition. Furthermore, we investigate the development and evolution of wrinkle patterns beyond the instability, showing different wrinkled configurations. We discover the existence of a multi-wavelength mode following the purely sinusoidal wrinkles and anticipating the kinked configuration of the tube.

Introduction.—Exerting bending loads on a thin-walled tube elastically deforms the tube by curving it. If bending increases, the curvature reaches a critical value where an instability takes place, in which the curvature is localized on small regions of the surface [1]. This phenomenon can be observed in the sudden formation of a kink by bending a drinking-straw (Fig. 1a).

Brazier studied the buckling of tubular shells subjected to bending, finding that the relation between torque and curvature is not monotonic [2]. A first type of instability is known as Brazier effect and is expected to occur at the curvature giving a maximum torque. Nonetheless, a second type of instability, known as the wrinkling or bifurcation instability, can occur at a torque (and curvature) lower than that expected by Brazier’s, which results in wave-like structures immediately before the formation of the final buckled shape [3]. Depending on the geometric and mechanical properties of the shell, different shapes are observed beyond the instability, ranging from kinked configurations to wrinkled or triangular (Yoshimura) patterns [4].

The formation of kinks or wrinkles in tubes subjected to bending loads is not restricted to the macroscale [5]. At the nanoscale, wrinkled and/or kinked structures have been observed in carbon nanotubes and microtubules [6–8]. It is therefore expected that instabilities should also occur at intermediate scales. Rod-shaped bacteria are an interesting example of thin-walled tubes at the microscale. Yet, bacterial cells present a remarkable distinction compared to the previous examples: the differential concentration of osmolites between the interior and the exterior of the bacteria results in significant internal (turgor) pressures [9], such that they are deformed by pressure akin to a party balloon (Fig. 1b). Notably, cylindrical thin shells subjected to pressures are common in biological systems, e.g., blood vessels or the absorbent hairs in the roots of plants [10, 11]. This situation is

in stark contrast with that typically found in engineering problems, e.g. pipes, where the large stiffness of the material prevents significant deformations [12, 13].

Here, we investigate the response of thin-walled pressurized tubes under bending loads. We develop a computational model permitting us to extract the mechanical response, and to contrast it with recent analytical formulas [14]. Furthermore, using a theoretical framework based on tension-field theory, we extend the characterization of the torque-curvature relation beyond the wrinkling point. We find that the results observed in the computational model are well described by our theoretical framework, including the expected curvature at wrinkling. Since the behavior of the system beyond the instability is challenging to describe analytically, we computationally characterize the properties of the wrinkles, their dependency on pressure, and how the wrinkled state evolves with additional bending post-buckling. We show that two different wrinkled states can be formed beyond the instability and prior to the final kinked configuration. In particular, we observe a sinusoidal regime with low amplitude wrinkles, followed by a multi-wavelength

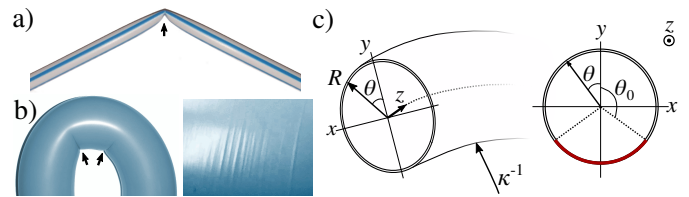


Figure 1. Buckling of thin tubes under bending loads. a) Buckled drinking straw. b) *left*. Buckling in a pressurized party balloon. Arrows highlight the buckled regions. *right*. Wrinkles observed at the bottommost side of a pressurized and bent party balloon, anticipating the buckling shown in the left panel. c) Geometric variables. The wrinkled area (red) spans the domain $\theta > \theta_0$ and $\theta < -\theta_0$, with $\theta \in [-\pi, \pi]$.

pattern including large amplitude wrinkles anticipating the kinked configuration.

Model.—We study tubes with unpressurized radius R_0 and length $L_0 \gg R_0$ described by a triangulated mesh with two flat lids that close the volume of the tube. The total energy of the system is given by $\mathcal{E} = \mathcal{E}_{\text{int}} + \mathcal{E}_{\text{ext}}$. The internal (mechanical) energy of the pressurized shell is given by $\mathcal{E}_{\text{int}} = \mathcal{E}_s + \mathcal{E}_b - pV$ where p is the pressure and V the enclosed volume [15]. The stretching and bending energies, \mathcal{E}_s and \mathcal{E}_b , are described by harmonic potentials and penalize in-plane and out-of-plane deformations of the surface (Secs. I-III of the Supplemental Material, [16]). This model maps to a continuum material [17]. Taking bacteria as inspiration, we use the characteristic 3D Young modulus E and thickness t of Gram negative cell walls [18]. The potential \mathcal{E}_{ext} penalizes the misalignment between the normal vectors of the lids with respect to defined target vectors. This term is introduced to induce the overall bending of the tube, acting as virtual hands. We determine the resulting configurations at a given pressure by minimizing \mathcal{E} at progressively increasing degrees of bending.

Results.—The buckling of a tube in the absence of pressure has been widely studied during the last century [1, 2]. Therefore, we used the unpressurized condition as a proof-of-principle of the ability of the computational model to produce well-established results. We find quantitative agreement with the response described in the literature for the torque-curvature ($M - \kappa$) curves as well as for the geometry/ovalization of the cross-section (with radii R_x and R_y), see Sec. IV of the Supplemental Material [16]. Furthermore, at the theoretically expected wrinkling curvature the shell collapses in a kinked configuration resembling that of bent drinking straws (Fig. 1a).

Having verified that the numerical model is consistent with established theoretical predictions, we investigate the much less studied response of tubes in a pressurized state. We study a regime of pressures leading to radial expansions in the range 1-10%. We find that after sufficient bending, the tube acquires a wrinkled configuration (Fig. 2, top rows). The onset of the wrinkling instability is marked by the sudden appearance of periodic structures at the bottom of the tube (Supplemental Material and Movies S1-S3, [16]). Contrary to what is observed at zero pressure, the wrinkled state persists with additional bending, developing a complex wrinkling pattern before collapsing into a kinked configuration where the curvature is highly localized (Figs. 2, bottom row). That is, the wrinkling transition is not concomitant with the kinking instability, as occurs at zero pressure. Furthermore, kinked tubes again develop sinusoidal wrinkles in the space between kinks, and this is observed for every pressure [20].

Next, we characterized the mechanical response to bending. From the torque-curvature curves we find that for low bending, M grows linearly with κ (Fig. 3a). The

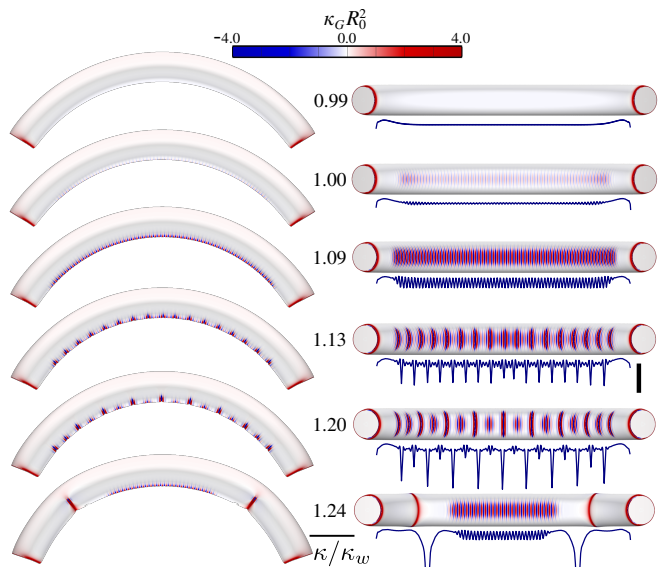


Figure 2. Wrinkle patterns during bending. Resulting configurations after the wrinkling transition for $\hat{p} \equiv pR/(Et) = 0.026$ at progressively increasing curvatures κ/κ_w from top to bottom, where κ_w is the curvature at the onset of wrinkling. The surface is colored according to Gaussian curvature, κ_G [19]. Blue continuous lines show the radius at the bottom of the tube R_y along the arc length of the tube. The scale bar indicates $R_y/R_0 = 0.05$. The pictures at $\kappa/\kappa_w = 1.13$ and $\kappa/\kappa_w = 1.20$ are representative examples of the system in the multi-wavelength state (MWS) at the low and high wavelength substates, respectively.

response continues until the tube develop wrinkles, from which point further bending results in sublinear increase of M with κ , eventually plateauing near the kinking instability. We determine the curvature and torque at the onset of wrinkling, κ_w and M_w as well as that at the onset of the kinking instability, κ_{kink} and M_{kink} (Fig. 3b). We find that the wrinkled state exists for a larger range of κ beyond the wrinkling transition for high p . As a result of the saturating behavior of the torque with κ , the difference in torque between M_w and M_{kink} is small and shows little dependency on p .

Recently, the mechanics of pressurized bent tubes has been studied analytically [14]. Here we further the understanding by including the response after the onset of wrinkling. To understand the mechanical response including the saturating post-wrinkling torque, we develop an analytical model using tension-field theory (TFT, [21]). The underlying assumption of TFT is that wrinkles accommodate extra area, relieving large negative stresses and minimizing the in-plane deformation energy. On the unwrinkled region of the tube we assume linear relations between the resultant membrane stress and the strains. On the wrinkled region of the tube, we follow a TFT framework where we assume that the formation of wrinkles suppresses further increase of compressive stress with bending. Thus, the lateral stress N_z remains constant at

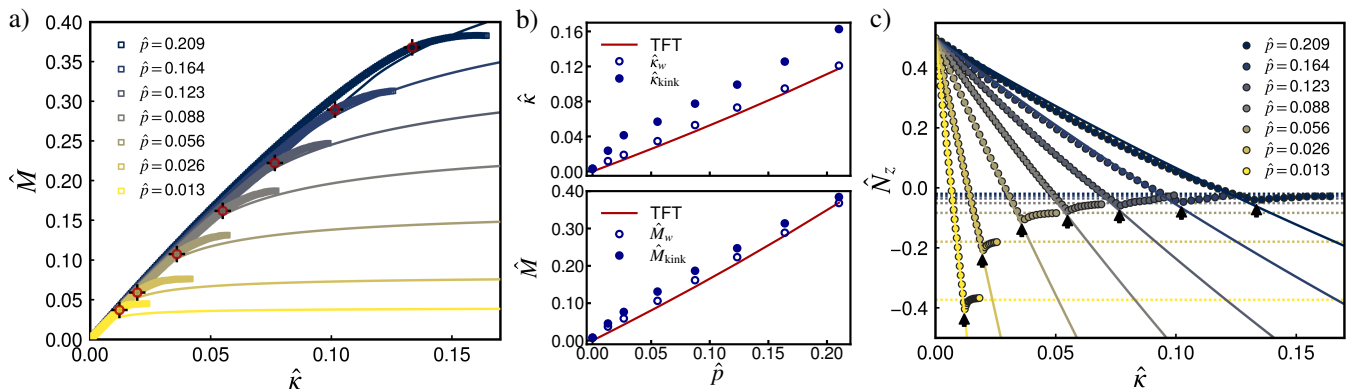


Figure 3. Mechanics of pressurized bent tubes. a) Torque and curvature. The observed buckling position for each pressure is indicated with red bullets. Theoretical predictions from the tension-field theory (TFT) are shown with continuous lines (Eqs. 3 and 4). b) Curvature (*top*) and torque (*bottom*) at the onset of wrinkling (open symbols) and at the kink instability (filled symbols). The continuous lines are the predictions for $\hat{\kappa}_w$ and \hat{M}_w from TFT ($\hat{\kappa}_w = \hat{p}/2$ and $\hat{M}_w = \pi\hat{p}/2$). c) Stress resultants. The dimensionless resultant stress is defined as $\hat{N} \equiv N/(pR)$. Longitudinal stress resultants \hat{N}_z on the inner-most region of the tube as a function of curvature $\hat{\kappa}$. Continuous lines are the predictions from Eq. 2. The critical stresses N_c are indicated with dotted lines (Eq. 1). The observed onset of wrinkling for each pressure is marked with a black arrow.

a critical compressive stress and the wrinkled region expands along the circumferential direction upon bending. The critical resultant membrane stress N_c at the onset of wrinkling in an unpressurized tube is given by

$$N_c = \frac{2}{R_\theta} \sqrt{BY}, \quad (1)$$

where R_θ is the circumferential radius of curvature at the position of maximal compression [22]. Though R_θ can depend on κ due to cross-section ovalization, our numerical results show that, at the range of p studied, cross-section deformations are greatly suppressed by the internal pressure [16]. Thus, we assume that the cross-section remains circular. Considering linear elasticity, the resultant stress on the inner-most part of the tube ($\theta = \pi$, Fig.1c) before wrinkling is

$$N_z = \frac{pR}{2} - EtRK, \quad (2)$$

where \mathcal{K} is the curvature of the medial axis, $\mathcal{K} \equiv \kappa/(1 - \kappa R)$. We calculate the stresses from the simulation and compare them to our predictions in Fig. 3c. We observe a linear decrease of N_z with κ , with values well-described by Eq. 2. N_z remains (mostly) constant with additional bending once the system wrinkles and the compressive stresses in the wrinkled configuration are in good agreement with the expected critical stress given by Eq. 1. We can also calculate the M - κ relationship within this model. For mathematical convenience, we approximate the critical wrinkling stress as zero, such that in the wrinkled region ($|\theta| > \theta_0$, where θ_0 stands for the limiting extension of the wrinkles in the circumferential direction, Fig. 1c) the resultant membrane stress in the longitudinal direction equals zero, $N_z = 0$. We obtain a

pressure-independent linear relation between torque and curvature prior to the onset of wrinkling (Fig. 3a):

$$\hat{M} = \pi\hat{\kappa}, \quad (3)$$

where we use non-dimensional variables defined as $\hat{\mathcal{K}} \equiv \mathcal{K}R$, $\hat{M} \equiv M/(EtR^2)$ and $\hat{p} \equiv pR/(Et)$. Beyond the wrinkling transition, we find

$$\hat{M} = \left[\theta_0 - \frac{\sin(2\theta_0)}{2} \right] \hat{\mathcal{K}}, \quad (4)$$

where θ_0 depends on p and \mathcal{K} , see Sec. VI of the Supplemental Material [16]. The torque-curvature relation for fixed p determined within this model is plotted and compared to the simulation results in Fig. 3a. The computational results and the theoretical model are in good agreement, including the saturation of M with additional bending past the wrinkling transition. In addition, Eq. 2 can be used to calculate the expected curvature at the onset of wrinkling under the assumption that $N_z = 0$, leading to $\hat{\kappa}_w = \hat{p}/2$. We obtain good agreement between the simulation results and the theoretical predictions for both $\hat{\kappa}_w$ and \hat{M}_w (Fig. 3b). In a previous work, we developed a model to predict the onset of wrinkling by considering the cross-section deformation and the small but non-zero values of N_c [14]. This allows for a precise determination of κ_w and M_w prior to the onset of wrinkling, in quantitative agreement with the results of the simulations at the lowest pressures. However, in contrast with TFT, the predictive power for the mechanical response beyond the wrinkling instability is weak. A detailed description of the model and its comparison with TFT and with simulation results can be found in Sec. VII of the Supplemental Material [16].

Following the characterization of the mechanical properties, we seek to determine the geometrical properties of the wrinkles. The amplitude of the wrinkles, A , is very small compared with R (Fig. 2). Fourier analysis reveals that at low κ/κ_w the pattern of wrinkles shows a unique wavelength. This is observed for both high and low p [16]. As κ/κ_w increases, we observe the sudden appearance of a multi-wavelength state (MWS), where evenly spaced high amplitude wrinkles are surrounded by minor wrinkles (Fig. 2). Although this occurs for both low and high p , the spatial distribution of the wrinkles varies with pressure. For low p , the wrinkles with the largest amplitude are flanked by wrinkles of smaller amplitude. The amplitude of the small wrinkles quickly decays with the distance to the major wrinkle [16]. This configuration resembles the profile of wrinkles observed in compressed thin sheets [23, 24]. As p increases, the space between the major wrinkles shows complex patterns of high frequency and small amplitude wrinkles (Fig. 2b and Supplemental Movies S1-S3 [16]).

In light of the relatively complex patterns observed for large κ , we focused our analysis on the major wrinkles with the largest amplitude. Sustained bending after the wrinkling instability results in a slow and sub-linear increase of A with κ (Fig. 4a). In the sinusoidal regime we do not observe a dependency of A on pressure and for every p , the transition to the MWS occurs when $A(\kappa)/R_0 \approx 0.02$. After this transition, the amplitude of the wrinkles increases suddenly, and additional bending results in a faster increase of A compared with that in the purely sinusoidal state.

We observe that the wavelength in the sinusoidal regime λ_{sin} does not change with bending (Fig. 4b). Despite the similarities in wrinkle morphology, the trend observed differs from that of confined thin sheets, where there is a consistent decrease of λ when compressed, though consistent with the theoretical predictions under a linear elasticity framework [25]. Furthermore, we observe that λ_{sin} decreases with pressure, while the compressive stresses at the onset of wrinkling are smaller for higher pressures (Fig. 3c) [16]. Interestingly, the MWS state contains two substates. The transitions are marked by an abrupt increase of λ , coincident with a rapid increase in A . Once in a given state, λ remains mostly constant with bending. Following the transition from the sinusoidal regime we observe a substate with a small wavelength $\lambda_1 > \lambda_{\text{sin}}$ (Fig. 2 and Fig. 4b). Sustained bending results in an abrupt transition to a substate with larger wavelength ($\lambda_2 > \lambda_1 > \lambda_{\text{sin}}$). At the largest pressures, this transition is marked by an increase of the amplitude A for some of the wrinkles simultaneous with a decrease of A for other wrinkles until their eventual disappearance (Supplemental Movie S3, [16]).

From examination of the wrinkles in the sinusoidal regime, we notice that the wrinkles do not only grow in amplitude but also in their extent along the circumfer-

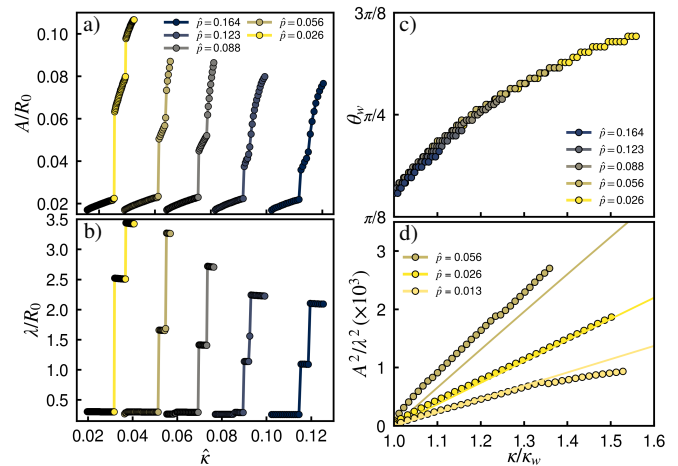


Figure 4. Geometrical properties of the wrinkles. a) Wrinkle amplitude A as a function of curvature $\hat{\kappa}$ after the wrinkling transition. b) Characteristic wavelength λ of the largest amplitude wrinkles for different pressures. The sudden jumps correspond to the transition to the MWS. c) Extent of the wrinkles in the sinusoidal regime measured along the polar angle $\theta_w \equiv \pi - \theta_0$ as a function of curvature. d) A^2/λ^2 relation as a function of curvature in the sinusoidal regime. The continuous lines are the predictions from Eq. 5.

ential direction (Supplemental Movies S1-S3, [16]). We determine the polar angle θ_w that results in the maximum curvature along the circumferential direction as a proxy for the extent of the wrinkles, where $\theta_w \equiv \pi - \theta_0$ [16]. We find that θ_w increases sublinearly with κ , resembling the response found for the wrinkle amplitude (Fig. 4d). We observe the same trend for all pressures and, remarkably, $\theta_w > 0$ at κ_w . The qualitative response of θ_w with κ is in accord with that predicted by TFT (Supplemental Material Sec. IV [16]). We observe that larger pressures transit to the MWS at lower θ_w , i.e., the transition to the multi-wavelength mode does not rely on a characteristic pressure-independent wrinkle width.

Intuitively, wrinkling is a mechanism preventing compressive stresses. Using an axial inextensibility condition for the inner-most area, building on the work of Ref. [5] we determine the following ratio between A and λ (Supplemental Material Sec. VIII, [16]):

$$\frac{A^2}{\lambda^2} = \frac{2 \sin(\theta_w)}{\pi^2 \theta_w} (\hat{\mathcal{K}} - \hat{\mathcal{K}}_w), \quad (5)$$

In contrast to [5], we limited the inextensibility condition to the wrinkled area defined by θ_w . The expression captures well the relation between the wrinkles amplitude (Fig. 4a) and wavelength (Fig. 4b) in the sinusoidal regime as a function of the bending curvature (Fig. 4d).

Conclusions.—We have developed a computational model to precisely characterize the mechanics and geometry of pressurized tubes subjected to bending. Using a simplified theoretical framework relying on tension-field

theory, we propose a model to characterize the torque-curvature curves beyond the wrinkling transition. We discover that the wrinkled state evolves with bending, encompassing first a purely sinusoidal regime which is subsequently followed by a multi-wavelength state anticipating the final buckling of the tube in a kinked configuration. In the sinusoidal regime, wrinkles undergo not only an increase in amplitude but also a concurrent expansion of their extent along the circumferential direction, θ_w . The value of θ_w decreases with pressure at the transition to the multi-wavelength state, while A is constant for all p . This suggests that a characteristic wrinkle amplitude is the main geometrical property triggering the transition to the multi-wavelength mode and the subsequent kinking of the tube.

We acknowledge Benny Davidovitch for insightful discussions and L. Mahadevan for pointing out Ref. [5]. This work was supported by Volkswagen Stiftung (A.A. and U.G.) and the Harvard Quantitative Biology Initiative and Grant NSF-1806818 (L.Q.). A.A. thanks the Clore Center for Biological Physics for their support.

-
- [1] C. R. Calladine, “The Brazier effect in the buckling of bent tubes,” in *Theory of Shell Structures* (Cambridge University Press, 1983) p. 595–625.
- [2] L. G. Brazier and R. V. Southwell, *Proceedings of the Royal Society of London. Series A* **116**, 104 (1927).
- [3] S. A. Karamanos, *Int. J. Solids Struct.* **39**, 2059 (2002).
- [4] A. Vaziri, *Thin-Walled Structures* **47**, 692 (2009).
- [5] L. Mahadevan, J. Bico, and G. McKinley, *Europhys. Lett.* **65**, 323 (2004).
- [6] O. Lourie, D. M. Cox, and H. D. Wagner, *Phys. Rev. Lett.* **81**, 1638 (1998).
- [7] S. Iijima, C. Brabec, A. Maiti, and J. Bernholc, *J. Chem. Phys.* **104**, 2089 (1996).
- [8] E. Memet, F. Hilitski, M. A. Morris, W. J. Schwenger, Z. Dogic, and L. Mahadevan, *eLife* **7**, e34695 (2018).
- [9] X. Yao, M. Jericho, D. Pink, and T. Beveridge, *J. Bacteriol.* **181**, 6865 (1999).
- [10] A. C. Burton, *Physiol. Rev.* **34**, 619 (1954).
- [11] C. Grierson, E. Nielsen, T. Ketelaarc, and J. Schiefelbein, *The Arabidopsis Book* **2014** (2014), 10.1199/tab.0172.
- [12] Y. Lin and S. Kyriakides, *Int. J. Solids Struct.* **51**, 599 (2014).
- [13] S. Kyriakides and E. Corona, *Mechanics of offshore pipelines: volume 1 buckling and collapse*, Vol. 1 (Elsevier, 2007).
- [14] L. Qiu, J. W. Hutchinson, and A. Amir, *Phys. Rev. Lett.* **128**, 058101 (2022).
- [15] C. L. Pastrana, L. Qiu, S. Armon, U. Gerland, and A. Amir, *Soft Matter* **19**, 2224 (2023).
- [16] See Supplemental Material at [URL_will_be_inserted_by_publisher](#) for additional details of the computational model, estimation of parameters and videos.
- [17] H. S. Seung and D. R. Nelson, *Phys. Rev. A* **38**, 1005 (1988).
- [18] X. Yao, M. Jericho, D. Pink, and T. Beveridge, *J. Bacteriol.* **181**, 6865 (1999).
- [19] M. Meyer, M. Desbrun, P. Schröder, and A. H. Barr, in *Visualization and Mathematics III*, edited by H.-C. Hege and K. Polthier (Springer Berlin Heidelberg, Berlin, Heidelberg, 2003) pp. 35–57.
- [20] Since the mesh model does not include long range interactions, the surface can intersect with itself near the kinks. We therefore focus our analysis on the regime before the appearance of kinks.
- [21] D. J. Steigmann and A. E. Green, *Proc. R. Soc. A: Math. Phys. Eng.* **429**, 141 (1990).
- [22] P. Seide and V. I. Weingarten, *J. Appl. Mech.* **28**, 112 (1961).
- [23] L. Pocivavsek, R. Dellsy, A. Kern, S. Johnson, B. Lin, K. Y. C. Lee, and E. Cerda, *Science* **320**, 912 (2008).
- [24] O. Oshri, F. Brau, and H. Diamant, *Phys. Rev. E* **91**, 052408 (2015).
- [25] F. Brau, H. Vandeparre, A. Sabbah, C. Poulard, A. Boudaoud, and P. Damman, *Nat. Phys.* **7**, 56 (2011).